ON THE DEVELOPMENT OF SPATIOTEMPORAL STRUCTURE IN A TWO-DIMENSIONAL TURBULENT JET

Yasuhiko Sakai, Nobuhiko Tanaka, Takehiro Kushida
Department of Mechano-Informatics and Systems,
Nagoya University
Furo-cho, Chikusa-ku, Nagoya, 464-8603, Japan
ysakai@everest.mech.nagoya-u.ac.jp, tanaka@sps.mech.nagoya-u.ac.jp
kushitk@mech.nagoya-u.ac.jp

INTRODUCTION

In recent years, the generation and collapse process of the coherent structure in a turbulent flow have been observed in many experiments and numerical simulations (see Holmes et al.(1996), Silva and Metatis(2002a) for example). Since these coherent structures cause the oscillation, the frictional drag and the sound noise, etc., the understanding of these physical characteristics is very important for industrial applications. In this study, we adopted a plane jet which is fundamental and easy to handle as a research subject of the coherent structure. As the experimental technique to extract the coherent structures, the Karhunen-Loève expansion (hereafter, called the KL expansion) which is also referred to as POD (Proper Orthogonal Decomposition) is an useful mathematical tool. It is known that the KL expansion can extract the spatial eigenfunctions(i.e., 'modes') which represent the coherent structures if they have a dominant percentage of the turbulent kinetic energy (Holmes et al., 1996). In our last paper (Sakai et al., 2002b), we reported the downstream change of distributions of the eigenvalues and the eigenfunctions in the cross-streamwise direction only by the KL expansion. In this paper, mainly by the combination of the KL expansion and the Fourier transform, the structure development of a plane jet has been investigated from a viewpoint of frequency space besides the physical space. Further, the shear-stress cospectrum and spatial correlation of velocity are examined and the jet structure is discussed from a viewpoint of these joint statistics.

SUMMARY OF THE COMBINED ANALYSIS OF THE KL EXPANSION AND THE FOURIER TRANSFORM

By the combination of the KL expansion and the Fourier transform, the orthogonal decomposition for both space and frequency can be perfomed (George(1990), Delville et al.(1991)). In this study, the KL expansion was made to the cross-streamwise direction (x_2 direction in figure 2) and the Fourier transform was applied to the time space.

The problem to solve may be written as follows:

$$\int_{\mathrm{I}} R(x_2, x_2', \tau)\psi^{(n)}(x_2', \tau)dx_2' = \hat{\lambda}^{(n)}(\tau)\psi^{(n)}(x_2, \tau), \quad (1)$$

$$R(x_2, x_2', \tau) = \left\langle u(x_2, t)u(x_2', t')\right\rangle, \quad (2)$$

where $\tau = t - t'$ is the time difference, $R(x_2, x_2', \tau)$ is the two-point correlation of the velocity component, i.e., u (the x_1-component, see figure 2), $\psi^{(n)}(x_2, \tau)$ is the eigenfunction in the (x_2, τ)space and $\hat{\lambda}^{(n)}(\tau)$ is the eigenvalue. Now we describe the time Fourier transform of R, $\psi^{(n)}$ and $\hat{\lambda}^{(n)}$ as Φ, $\phi^{(n)}$ and $\lambda^{(n)}$, respectively. For instance, $R(x_2, x_2', \tau)$ is transformed as follows,

$$\Phi(x_2, x_2', f) = \int R(x_2, x_2', \tau)e^{-i2\pi f\tau}d\tau, \quad (3)$$

where f is the frequency and $\Phi(x_2, x_2', f)$ becomes a cross-spectrum. After performing the time Fourier transform of equation (1), we obtain the following equation

$$\int_{\mathrm{I}} \Phi(x_2, x_2', f)\phi^{(n)}(x_2', f)dx_2' = \lambda^{(n)}(f)\phi^{(n)}(x_2, f). \quad (4)$$

Since in the present experiments the velocity field was measured by the hot-wire probes, the kernel in equation (4) can be known only at discrete positions where probes are set up. Then the equation (4) can be replaced by the discrete eigenvalue problem of the matrix Φ which has the eigenvalue $\lambda^{(n)}$ and the eigenfunctions $\phi^{(n)}$. Here we must solve the complex eigenvalue problem because each element of the matrix Φ is a complex number. But since Φ is the Hermitian matrix, the eigenvalues are real numbers and the eigenfunctions becomes complex functions. The KL expansion provides an important property that the turbulent kinetic energy can be expressed as the sum of the eigenvalues, i.e.,

$$E = \int_{\mathrm{I}} \langle u^2 \rangle \, dx = \sum_{n,f} \lambda^{(n)}(f). \quad (5)$$

Therefore the eigenfunction with the maximum eigenvalue contains the largest amount of kinetic energy. Usually, according to the magnitude of the eigenvalue, the eigenvalue and eigenfunction are ordered such that $(\lambda^{(1)}, \phi^{(1)}), (\lambda^{(2)}, \phi^{(2)}), \cdots, (\lambda^{(n)}, \phi^{(n)})$. Using eigenvalues $\lambda^{(n)}$ and eigenfunctions $\phi^{(n)}$ obtained by this analysis, the power spectrum S is reconstructed from the following equation

$$S(x_2, f) = \sum_{n=1}^{\infty} \lambda^{(n)}(f)|\phi^{(n)}(x_2, f)|^2. \quad (6)$$

EXPERIMAENTAL APPARATUS AND CONDITIONS

Figure 1 shows the sketch of the experimental apparatus. The jet was issued from the skimmer which has the hight of d = 12mm and the aspect ratio of 19.7 (see figure 2). The Reynolds number $Re(= U_0 d/\nu)$ is adjusted to 16,000 where the exit velocity U_0 is about 20m/s. For the velocity measurements, the X-type hot wire probe was used. The tungsten wire of 5μm was attached with the thin tip of the piano wire of a diameter of 0.5mm by means of the spot welding. Figure 2 shows the coordinate system. The streamwise (downstream) coordinate is x_1, the vertical

(cross-streamwise) coordinate is x_2 and the spanwise coordinate is x_3. Firstly the one-point measurements have been made along the jet centerline and in the cross-streamwise direction at several streamwise locations, i.e., at $x_1/d = 1.0$, 2.0, 3.0, 4.0, 5.0, 6.0, 8.0, 10.0, 15.0, 20.0, 25.0, 30.0, 35.0, 40.0. Next the two-point measurements have been performed, and the data examined by caluculating the spatial correlation or making the combined analysis of the KL expansion and the Fourier transform. The locations of the two-point measurements are $x_1/d = 2.0, 3.0$ (in the potential core region), 4.5 (in the beginning of the interaction region), 6.0 (in the end of the interaction region), 10.0 and 20.0 (in the self-preserving region). The 21 measurement points are set up in one section and the interval of each measurement points is adjusted to $2.5b/10$ (b:half-width of the radial profile of the mean streamwise velocity). The cross-spectrum is calculated from the discrete finite samples by means of FFT. Because of the sampling frequency 10kHz, the frequency domain of the cross-spectrum is limited to 5kHz of the Nyquist frequency. The frequency resolution Δf is about 2.4Hz which is obtained by deviding the Nyquist frequency into $2048(=2^{11})$ parts. Consequently, the eigenfunctions $\lambda^{(n)}(f)$ of 2047 except for f =0.0Hz are caluculated from the cross-spectrum matrix of 21×21.

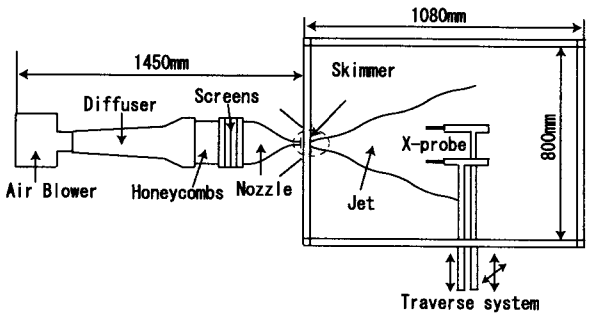

Figure 1: Experimental apparatus

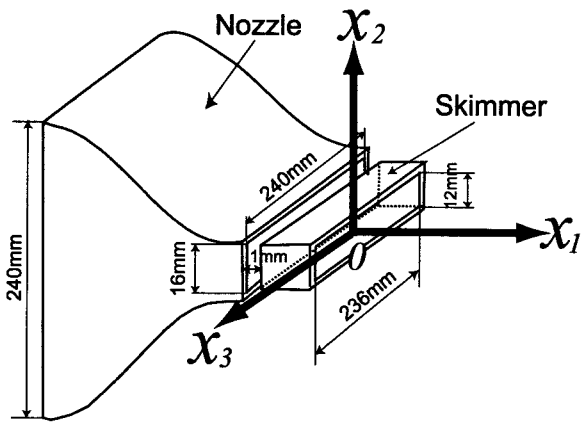

Figure 2: Coordinate system

FUNDAMENTAL CHARACTERISTICS OF A PLANE JET IN PRESENT EXPERIMENTS

The first moment (the mean streamwise velocity U and the mean cross-streamwise velocity V) and the second moment (the streamwise r.m.s. velocity u' and the cross-streamwise r.m.s. velocity v') of the jet velocity field are investigated. Although these figures are not shown here, we ascertained that the centerline streamwise mean velocity U_m for $x_1/d > 6.0$ is approximated by

$$\left(\frac{U_m}{U_0}\right)^{-2} = 0.13\left(\frac{x_1}{d} + 3.4\right). \tag{7}$$

Then the half-width b for $x_1/d > 6.0$ is approximated by

$$\left(\frac{b}{d}\right) = 0.11\left(\frac{x_1}{d} + 2.6\right). \tag{8}$$

The cross-streamwise profiles of the first moment and the second moment show the similarity for $x_1/d > 6.0$ and $x_1/d > 10.0$, respectively. Figure 3 shows the profile of Reynolds stress $\overline{uv}$. The profile becomes nearly similar for $x_1/d > 10.0$ and the peak value exists at $x_2/b \sim \pm 0.65$.

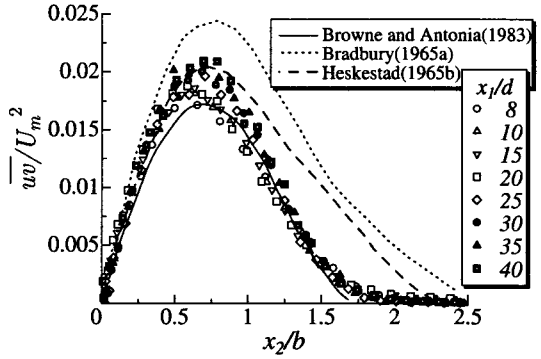

Figure 3: Reynolds stress profiles

ANALYSIS OF THE JOINT STATISTICS

Shear-stress cospectrum

The cross-spectrum $S_{uv}(f)$ for the Reynolds shear-stress $\overline{uv}$ is generally a complex function

$$S_{uv}(f) = K_{uv}(f) - iQ_{uv}(f), \tag{9}$$

where $K_{uv}(f)$ is a real part and $Q_{uv}(f)$ is an imaginary part, and then $K_{uv}(f)$ and $Q_{uv}(f)$ are respectively called a cospectrum and a quadrature spectrum. Figure 4 shows the downstream variation of the shear-stress cospectrum near the position of the peak of Reynolds stress and near the centerline at several streamwise locations. The ordinate is normalized by the u', v' and the integral time scale T_{uI} of u. The cospectrum near the position of the peak of the Reynolds stress exhibits apparently the -7/3 power range at $x_1/d = 6.0$, but the -7/3 power law becomes obscure at $x_1/d = 20.0$ and 40.0. On the other hand, the cospectrum near the centerline shows almost the similar distribution at each downstream location and does not exhibit the -7/3 power law. This reason is that the -7/3 power range appears only when both the energy-dissipation rate and the mean-shear rate $\partial U/\partial x_2$ have played important roles in characteristics of the turbulent field. The influence of the local mean-shear will become small in the larger downstream

region and the mean-shear has not any explict effect on the cospectrum at $x_1/d \sim 40.0$. It is a future subject to investigate the relationship between the -7/3 power law and the structure of a plane jet.

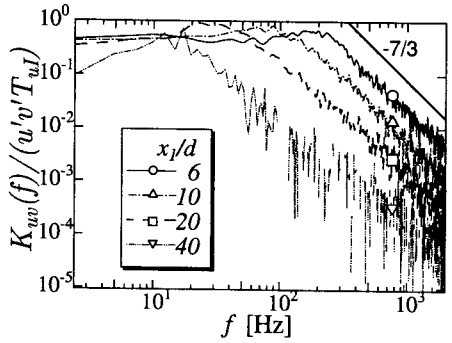

(a)at the position near the Renolds stress's peak

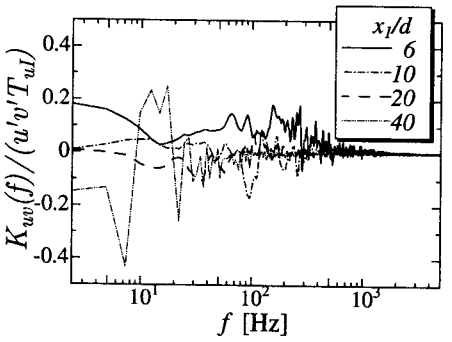

(b)at the position near the jet centerline

Figure 4: Downstream variation of the cospectrum $K_{uv}(f)$

Spatial correlation of the velocity

Figure 5 shows the spatial correlation coefficient of the velocity in three regions. The spatial correlation coefficient is defined by the following equation

$$R_{u_iu_i}(r) = \frac{\overline{u_i(x_2,t)u_i(x_2',t)}}{\sqrt{\overline{u_i^2(x_2,t)}}\sqrt{\overline{u_i^2(x_2',t)}}}, \qquad (10)$$

where $r = x_2' - x_2$ is the probe interval, and i is 1 or 2 (the summation convection is not used here). We also u and v instead of u_1 and u_2. The contour lines in this figure are drawn for every 0.1 and show 1.0 in the probe's position, where the abscissa and ordinate take the same value. It is found that the correlation patterns are different in each region. Since the pattern in the interaction region (figure 5(b)) has both features of the potential core region and the self-preserving region, it turns out well that this location is in the transition region. On opposite sides of the jet centerline, the u-correlation R_{uu} becomes negative and the v-correlation R_{vv} becomes positive in the self-preserving region (figure 5(c)). This feature in the self-preseving region has been also confirmed by other investigators and this can be attributed to the 'jet flapping phenomenon' (antisymmetric array of counter-rotating vortices). The experimental results also show that the values of R_{uu} at $(x_2/b, x_2'/b) = (\pm 0.5, \mp 0.5)$, $(\pm 0.75, \mp 0.75)$ and $(\pm 1.0, \mp 1.0)$ become negative at $x_1/d = 10.0$ and the values at $(x_2/b, x_2'/b) = (\pm 0.5, \mp 0.5)$ and $(\pm 0.75, \mp 0.75)$ become negative at $x_1/d = 20.0$. So, we invetigated the downstream variation of spatial correlation R_{uu} and R_{vv} at $(x_2/b, x_2'/b) = (\pm 0.5, \mp 0.5)$ and $(\pm 0.75, \mp 0.75)$ (figure 6). It is found that the spatial correlation in the potential core region takes the sign opposite to the one in the self-preserving region. So it is considered that the counter-rotating vortices are formed symmetrically for the jet centerline in the potential core region. Further, in the distribution of u-spatial correlation in the potential core region (left side of figure 5(a)), the lobes with the negative peak near $(x_2/b, x_2'/b) = (\pm 0.25, \pm 1)$ and $(\pm 1, \pm 0.25)$ are observed . These negative peakes are caused by the same vortex structure which has the larger speed near the jet centerline and the smaller speed at an outer edge.

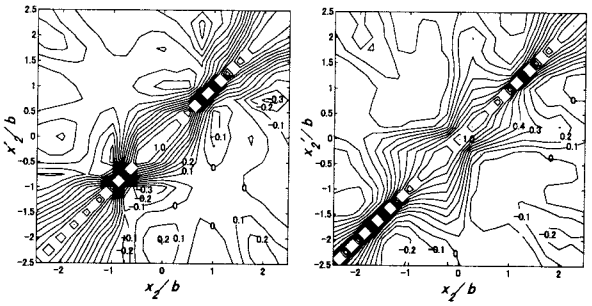

u-spatial correlation R_{uu} v-spatial correlation R_{vv}

(a) in the potential core region $(x_1/d = 2.0)$

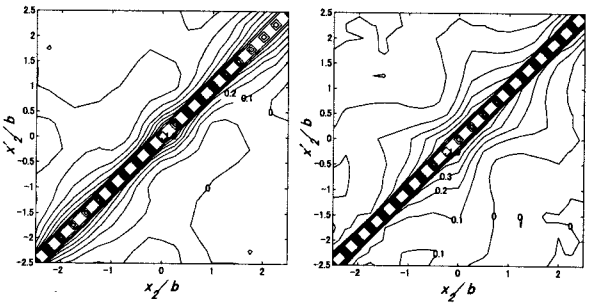

u-spatial correlation R_{uu} v-spatial correlation R_{vv}

(b) in the interaction region $(x_1/d = 4.5)$

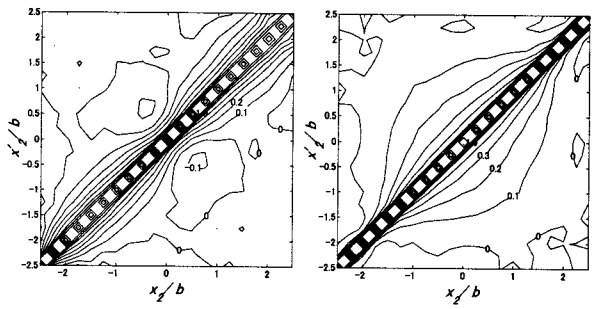

u-spatial correlation R_{uu} v-spatial correlation R_{vv}

(c) in the self-preserving region $(x_1/d = 20.0)$

Figure 5: Downstream variation of spatial correlation $R_{u_iu_i}$

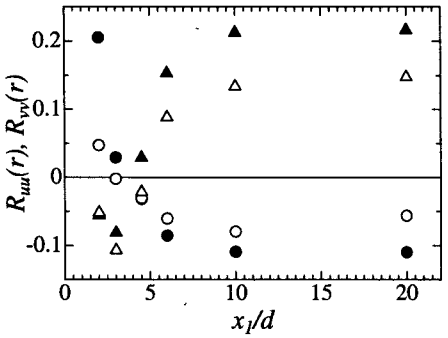

Figure 6: Downstream variation of spatial correlations on opposite sides of the jet centerline. ● , R_{uu} at $(x_2/b, x_2'/b) = (\pm 0.5, \mp 0.5)$; ○ , R_{uu} at $(\pm 0.75, \mp 0.75)$; ▲ , R_{vv} at $(\pm 0.5, \mp 0.5)$; △ , R_{vv} at $(\pm 0.75, \mp 0.75)$.

THE COMBINED ANALYSIS OF THE KL EXPANSION AND FOURIER TRANSFORM

Eigenvalues

Figures 7 and 8 show the downstream variation of eigenvalue distribution. The distribution of the potential core region is different from ones of the other regions. In the potential core region the contributions of the first mode and second mode are very large as compared to ones in other regions, and the sum of first three modes for u and v reaches about 80% and 90%, respectively. Thus first a few modes can make the dominant contribution to the fluctuation energy. This fact suggests that the Galerkin projection of these first a few modes into the Navier-Stokes equtions could provide a model that can capture the large-scale dynamics of a plane jet (Aubry(1988), Ukeiley and Glauser(1995)). Namely this analysis method has the possibility for constructing a low dimensinal dynamical model of a plane jet. Figures 9 and 10 show the downstream variation of eigenvalues $\lambda_u^{(1)}(f)$ and $\lambda_v^{(1)}(f)$ for the first mode. The ordinates are normalized by the sum of all eigenvalues $\sum \lambda_u^{(n)}(f)$ and $\sum \lambda_v^{(n)}(f)$. So the value of the ordinate shows the contribution of each frequency to the fluctuation energy, so that it has the same meaning as the normal power spectrum. In this study, the frequency distribution of the eigenvalue is called the 'eigenvalue spectrum'. From figure 9 and 10, it is noticed that the downtream variations of the eigenvalue spectra are very similar to the downstream variations of the power spectra of the u and v component (see figure 12), i.e., as the location becomes far from nozzle, the contribution of the low frequency range grows and the contribution of the high frequency range decreases. Therefore it turns out that the large-scale (low frequency) structure becomes dominant in the first eigenvalue spectrum as going to the more downstream position. Further, it is also noticed that the -5/3 power law appears like the power spectrum in the self-preserving region.

Eigenfunctions

Figure 11 shows the space-frequency distribution of the first eigenfunction $\phi^{(1)}(x_2, f)$ in three regions. The two lateral axs show the frequency and x_2 normalized by the half-width b, respectively. The vertical axis takes an absolute value of the first eigenfunction because the eigenfuction is a complex function. The first mode contains the largest amount of kinetic energy and the contributions of the energy to $< u^2 >$ and $< v^2 >$ are respectively 43.7%, 52.3% at

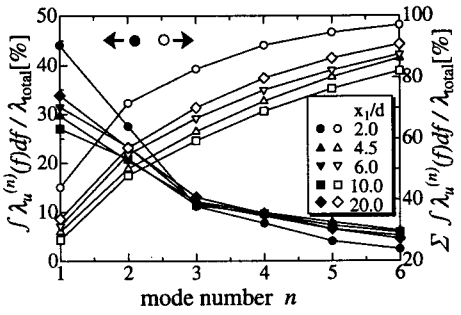

Figure 7: The eigenvalue for u-mode

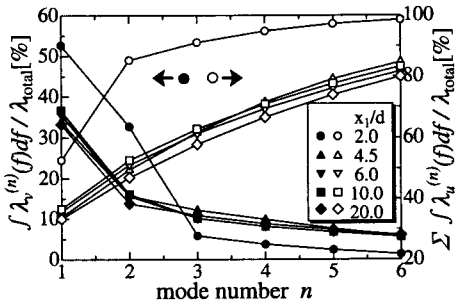

Figure 8: The eigenvalue for v-mode

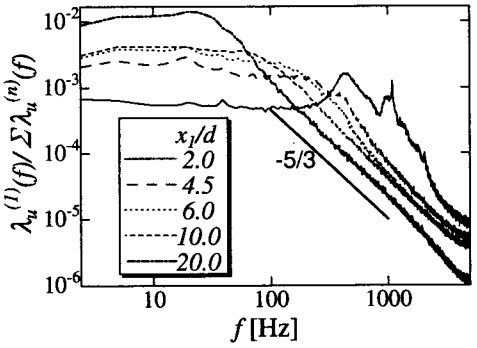

Figure 9: The eigenvalue for the first u-mode

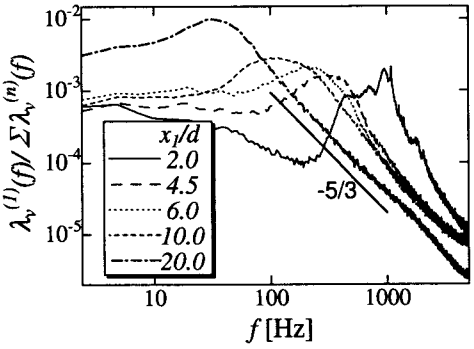

Figure 10: The eigenvalue for the first v-mode

$x_1/d = 2.0$, 28.6%, 32.7% at $x_1/d = 4.5$ and 33.6%, 31.6% at $x_1/d = 20.0$. In the potential core region, the distribution has the peaks at $|x_2/b| = 0.5 \sim 0.7$ with respect to space, but it has the peaks at various places with respect to the frequency. Its reason seems to be that the vortex structures produced in the potential core region have not interfered mutually yet. In the interaction region, many large peaks appear along the frequency axis in the high frequency range, and it is thought that many small-scale structures are generated. Since the contribution of energy in high frequency range is very small as shown in the first eigenvalue spctra (figures 9 and 10), the structures in this range contain very small energy. However, it is found that the form of overall structure becomes clearer than the one in the potential core region, so it seems that in the interaction region the reconstruction of vortex structures has been progressed and the stable structures have been formed in the self-preserving region. In the self-preserving region, the distribution in the high frequency range show one peak near centerline with respect to the space, while in the interaction region the distribution has two peaks. In the self-preserving region, while the distribution for u and v are different in the low frequncy range, they show almost the same distribution in the high frequncy range. It is supposed that this should be related with the local isotropy in the high frequncy range.

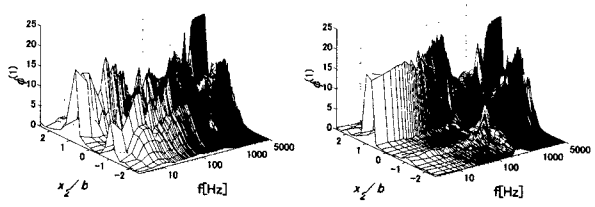

u-mode v-mode

(a)in the potential core region $(x_1/d = 2.0)$

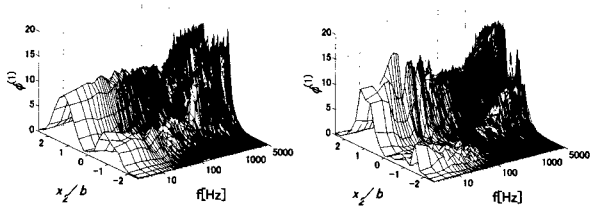

u-mode v-mode

(b)in the interaction region $(x_1/d = 4.5)$

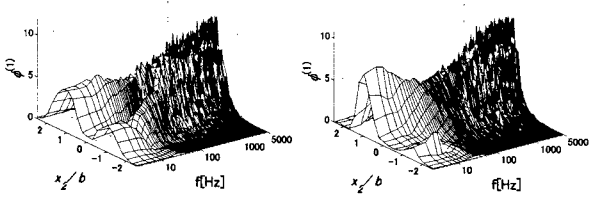

u-mode v-mode

(c)in the self-preserving region $(x_1/d = 20.0)$

Figure 11: Downstream variation of the space-frequency distribution of the first eigenfunction

RECONSTRUCTION OF THE POWER SPECTRUM

Using eigenvalues $\lambda^{(n)}(f)$ and eigenfunctions $\phi^{(n)}(x_2, f)$ obtained by the combined analysis of the KL expansion and Fourier transform, the power-spectrum $S(x_2, f)$ can be reconstructed from equation (6). Figure 12 shows the reconstructed spectrum at $x_2/b = +0.75$ (at the position near the peak of the Reynolds stress) in three regions. In this figure, 'sum of 1st mode' denotes the spectrum which is reconstructed only by the first mode, and 'sum of 3rd modes' denotes the spectrum which is reconstructed by the first three modes. It is found that the reconstruction is efficiently perfomed in the range that the original spectrum takes a big value. This shows very well the property of the KL expansion by which the flow structure is reconstructed in the order of the larger energy. In the potential core region, since the contributions of the energy for $< u^2 >$ and $< v^2 >$ are respectively 82.5% and 90.0%, the profile of 'sum of 3rd modes' reproduces mostly the profile of original spectrum. It turns out that this analysis method is more efficient to extract the flow structure with a peak in the spectrum like in the potential core region, more efficiently than the one with the smooth spectrum like in the self-preserving region. In the interaction region and the self-preserving region, both profiles of 'sum of 1st mode' and 'sum of 3rd modes' show the fluctuation in high frequency range. The reason is that the reconstruction is hardly performed in high frequency range because the contribution from the sum of the first three modes reaches about 60∼70% and the energy is mainly used for reconstruction of the structure with the large spectrum value. Therefore in the self-preserving region of a plane jet, it is expected that the fluctuation energy of the small-scale structures contain about 30∼40%.

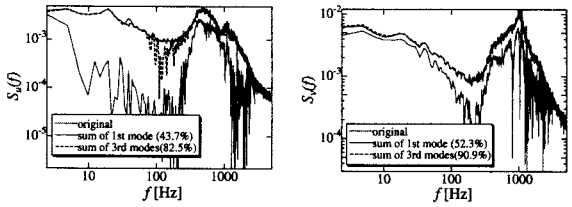

(a)in the potential core region $(x_1/d = 2.0)$

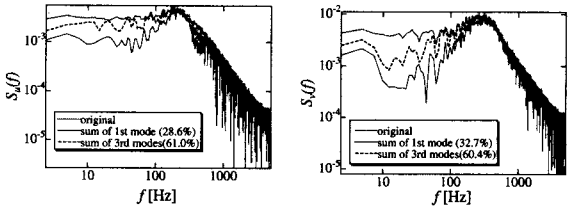

(b)in the interaction region $(x_1/d = 4.5)$

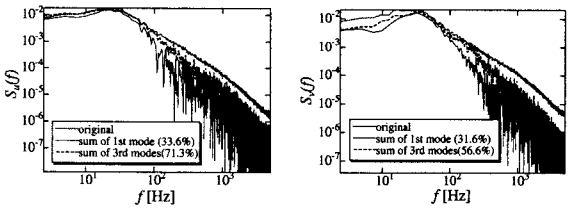

(c)in the self-reservating region $(x_1/d = 20.0)$

Figure 12: Downstream variation of the reconstructed spectrum $(x_2/b = +0.75)$

CONCLUSIONS

(1) In the interaction region, the shear-stress cospectrum near the position of the peak of the Reynolds stress exhibits the -7/3 power law, but the one near the centerline does not exhibit the -7/3 power law. The influence of the local mean-shear becomes small in the far downstream region, so the cospectrum near the position of the peak of the Reynolds stress at $x_1/d \sim 40.0$ does not exhibit the -7/3 power law.

(2) The distributions of the spatial correlation of the velocity are different in three regions. On opposite sides of the jet centerline, in the potential core region the u-correlation R_{uu} becomes positive and the v-correlation R_{vv} becomes negative, and in the self-preserving region the R_{uu} becomes negative and the R_{vv} becomes positive. These results mean that the counter-rotating vortices are formed symmetrically for the jet centerline in the potential core region and these vortex structures are redistributed in the form of the antisymmetric array in the self-preserving region.

(3) From the combined analysis of the KL expansion and Fourier transform, the following conclusions are obtained.

   (a) From the downstream variation of the first eigenvalue spectrum, it is found that the contribution of the low frequency range grows and the one of the high frequency range decreases as the downstream location becomes far from nozzle. Therefore it turns out that the large-scale (low frequency) structure becomes dominant in the first eigenvalue spectrum as going to the more downstream position.

   (b) In the self-preserving region, the space-frequency distributions of the first eigenfunctions of u and v are different in the low frequncy range. However they show almost the same distribution in the high frequncy range.

   (c) From the reconstruction of the power spectrum, it is found that the reconstruction of the structure is performed in the order of the larger fluctuation energy (the large value of the original's spectrum). In the self-preserving region, the reconstruction is hardly performed in the high frequency range because the contribution from the sum of the first three modes is about 60∼70%. Therefore in the self-preserving region of a plane jet, the fluctuation energy of about 30∼40% is contained in the small-scale structures.

RERERENCE

Aubry, N., Holmes, O., Lumley J. L., and Stone, E., 1988, "The dynamics of coherent structures in the wall region of turbulent shear layer", *J. Fluid Mech.*, Vol.192, pp.115-175.

Bradbury, L. J. S., 1965a, "The structure of a self-preserving turbulent plane jet", *J. Fluid Mech.*, Vol.23, part1, pp.31-64.

Browne, L. W. B. and Antonia, R.A., 1983, "Measurements of turbulent Prandtl number in a plane jet", *Trans. Am. Soc. Mech. Engrs C: J. Heat Transfer,* Vol.105, pp.663-665.

Delville, J., Bellin, S., and Bonne, J. P., 1991, "Use of the proper orthogonal decomposition in a plane turbulent mixing layer, in *Turbulent and Coherent Structures",* KLUWER ACADEMIC PUBLISHERS, pp.75-90.

George, W. K., 1990, "Insight into the Dynamics of Coherent Structures from a Proper Orthogonal Decomposition in a plane turbulent mixing layer, in *NEAR-WALL TURBULENCE",* KLUWER ACADEMIC PUBLISHERS, pp.75-90.

Heskestad, G., 1965b, "Hot-wire measurements in a plane turbulent jet", *Trans. Am. Soc. Mech. Engrs E: J. Appl. Mech.,* Vol.32, pp.721-734.

Holmes, P., Lumley J. L., and Berkooz, G., 1996, "Turbulence, Coherent Structures, Dynamical System and Symmetry", Cambridge Univ. Press.

Sakai, Y., Tanaka, N., and Kushida, T., 2002b, "A Study on the Development of Turbulent Structure in a Plane Jet," *Proc. of the 5th JSME-KSME Fluids Engineering Conference,* Nagoya, CD-ROM, Paper No.09j-09, pp.1-6.

Silva, C. B. da, and Metatis O., 2002a, "On the influence of coherent structures upon interscale interactions in turbulent plane jets", *J. Fluid Mech.,* Vol.473, pp.103-145.

Ukeiley, L., and Glauser, M., 1995, "Dynamics of large-scale structures in a plane turbulent mixing layer", *Rep.* MAE-311,Department of Mechanical and Aeronatural Engineering, Clarkson University.